EUROPEAN ORGANIZATION FOR NUCLEAR RESEARCH

POLARIZATION IN ELASTIC K^+p SCATTERING BETWEEN 0.86 GeV/c AND 1.45 GeV/c: RESULTS AND PHASE-SHIFT ANALYSIS

S. Andersson*), C. Daum, F.C. Erné**), J.P. Lagnaux***), J.C. Sens**), F. Udo**) and F. Wagner

CERN, Geneva, Switzerland

ABSTRACT

Polarization and differential cross-section data at 0.86, 0.97, 1.09, 1.37, and 1.45 GeV/c are presented. An energy-independent phase-shift analysis from threshold up to 1.45 GeV/c using random searches at 19 momenta and the shortest path method to link solutions at different momenta, yields three solutions. One of these is unlikely; the other two coincide up to 0.86 GeV/c, and both show an anticlockwise half circle in the P_3 wave.

Submitted to the

Lund International Conference on Elementary Particles

Geneva - 20 June 1969

---

*) Visitor from the Institute of Physics, University of Lund, Sweden.

**) Visitor from the Foundation for Fundamental Research of Matter (F.O.M.), The Netherlands.

***) Visitor from the Institut Interuniversitaire des Sciences Nucléaires, Bruxelles.

1. INTRODUCTION

The question of the possible existence of resonances in the K^+p system in the mass region around 2 GeV is still under discussion. Thus far every attempt to establish the existence of Z*'s has failed. Phase-shift analyses[1,2] of the elastic K^+p reaction have been hampered greatly by the absence of accurate polarization data. Recently, a resonant solution found by Lea et al.[2] has been eliminated by a polarization measurement at 1.22 GeV/c [3].

In this contribution we present further polarization data, and also differential cross-section data at 0.86, 0.97, 1.09, 1.37, and 1.45 GeV/c. We have made an energy-independent phase-shift analysis on these and other available data from threshold up to 1.45 GeV/c. We have used the shortest path method to select the most probable solutions of each energy. In this way three different solutions survive, one of which, solution III, is definitively inferior to the other two. Solutions I and II are both continuations of solution A_I- of Bland et al.[1]. The P_3 amplitude in solutions I and II shows the onset of a resonant-like behaviour; however without more accurate data on both differential cross-sections and polarizations above 1.5 GeV/c no further conclusion can be drawn.

2. POLARIZATIONS AND DIFFERENTIAL CROSS-SECTIONS

The polarization and differential cross-section data have been taken in an unseparated beam by recording coincidences between elastically scattered kaons and recoil protons in counter hodoscopes placed in the horizontal plane around a polarized target. In this experiment a butanol target[4] (polarization 35%) has been used for the first time. The polarization direction was changed every 10 hours. The incoming kaons were identified with a Cerenkov counter and time-of-flight measurements over an 11 metre flight path. The residual contamination due to incoming protons in the beam (3-12%) was subtracted out by means of pp data taken separately. Furthermore, these proton data provided a check on the measured target polarization, since accurate pp polarization data are available in the literature. In the region where the scattered kaons could not be distinguished from the recoil protons by angle measurements alone, the identification followed from measurement of the flight time between the polarized target and the counter hodoscope. An on-line computer monitored the apparatus and preselected the data.

Background events, mostly due to bound protons in the target, were subtracted out after extrapolating into the elastic peaks the distribution of non-coplanar events measured simultaneously. The assignment of centre-of-mass angles and differential solid angles followed from straightforward kinematic calculations, completed by Monte Carlo calculations for scattering in the near-forward direction.

The results are shown in Figs. 1 and 2, and in Tables 1-6. The polarization data at 1.22 GeV/c have been published elsewhere[3]; they are included for completeness.

3. K^+p PHASE-SHIFT ANALYSIS FROM THRESHOLD TO 1.45 GeV/c

The phase-shift analysis has been performed by using the CERN II program[5] previously employed in the analysis of πN elastic data and in associated production of $K\Lambda$.

As input data we used polarization, differential cross-section[6], inelastic cross-section[6], and total cross-section[7] data at 19 momenta, between 0.14 and 1.45 GeV/c, and real parts of the forward scattering amplitude from dispersion relation fits[8].

From 0.14 to 0.64 GeV/c, only S- and P-waves have been assumed. Above 0.64 GeV/c both elastic and inelastic S-, P-, and D-waves have been admitted. It has been checked that at 1.45 GeV/c, F-waves are compatible with zero, and that their inclusion does not alter the results.

The search has been started by finding 200 different solutions at each energy. "Solution" we call every set of partial waves giving a reasonable value of χ^2 [Prob. $(\chi^2) > 10^{-3}$]. This corresponds in nearly all cases to a true minimum of χ^2. "Different" depends on the distance criterion given by

$$D = \sum_{\ell,j} \left| f^{(1)}_{\ell,j} - f^{(2)}_{\ell,j} \right|^2 (j + 1/2) \qquad (1)$$

Here the $f_{\ell,j}$ are the partial wave amplitudes. The minimum distance is required to be such that after 300 or more random searches a saturation becomes apparent. From experience it is expected that no qualitatively different solutions have been missed after 300-400 random trials.

In Fig. 3 we show the areas in the Argand diagrams covered by the solutions at 0.86 GeV/c. At this momentum 470 random trials result in 200 solutions, of which only two are genuinely different, due to the small inelasticity (σ_{inel} = 1.24 mb, σ_{tot} = 13.5 mb). At higher momenta the number of genuinely different solutions increases, even at momenta where accurate polarization data are available. In Fig. 4 similar areas are shown for the solutions at 1.22 GeV/c (obtained after 460 random trials). Here one distinguishes six regions of solutions. At momenta where no polarization data are available, no obvious grouping is apparent.

The "shortest path" method of Berkeley[9] has been used to link the solutions at the different momenta. In this method the result can depend on the distance criterion and on the starting momentum. We have chosen a zero solution at threshold for shortest paths upwards and all solutions at the highest momentum for shortest paths going downwards in momentum. Instead of the distance formula (1) we can also use a "smoothness condition" in the momentum transfer t [10]:

$$D = \sum_{t_i} \left\{ \left| f^{(1)}(t_i) - f^{(2)}(t_i) \right|^2 + \left| g^{(1)}(t_i) - g^{(2)}(t_i) \right|^2 \right\} \exp(\alpha t_i) , \qquad (2)$$

where f and g are the non-flip and spin-flip amplitudes at five t values between 0 and -1 GeV/c^2. The exponential weight factor has been chosen such that the distance criterion is about equally sensitive in the whole region of t covered by the data.

Of the 200 shortest paths possible, not more than five are continued through the entire range of momenta. Of these five only three (marked I, II, and III in the following discussion) are qualitatively different. This result turns out to be independent of the distance criterion (1) or (2). Only the choice of the starting momentum gives a difference. Shortest paths going upwards in momentum contain all three types of solutions; downwards only solution II occurs. In Figs. 5-9 and Table 7 the three solutions are indicated for every partial wave.

Solutions I and II are equal up to 0.86 GeV/c and coincide there with the repulsive S-wave solution (A_I-) of Bland et al.[1]. Solutions I and II branch out at 0.86 GeV/c, where the inelastic cross-section begins to rise. Above this momentum, the S_1-wave (see Fig. 5) becomes strongly inelastic in solution I, but remains nearly elastic in solution II. The rapidly moving S_1 phase suddenly stops in solution II and reverses direction. In doing so, it describes a small counter clockwise loop of a size compatible with uncertainties in the individual solutions. The S_1 wave in solution III remains zero up to 0.81 GeV/c and then jumps to -20° at 0.86 GeV/c.

The P_1 wave (Fig. 6) remains elastic in all three solutions. Again the phase of solution III jumps at 0.86 GeV/c (first polarization data) causing a hairpin structure in this wave.

In contrast to the P_1-wave, the P_3-wave (Fig. 7) becomes inelastic in all solutions from 0.86 GeV/c onward, as soon as the inelastic cross-section rises. Below 0.86 GeV/c the P_3-wave is attractive in solutions I and II, repulsive in III.

The D_3-wave (Fig. 8) remains small in all solutions. The D_5-wave (Fig. 9) remains zero up to 0.86 GeV/c in solutions I and II, and becomes absorptive above this momentum. In solution III the D_5-wave is attractive up to 0.86 GeV/c.

Solution III can be regarded as unlikely, because in this solution the S_1-wave remains zero up to 0.81 GeV/c and hence the isotropic behaviour of the differential cross-section outside the Coulomb region at low momenta would then have to be accounted for by a combination of higher waves. Also the hairpin structure in the P_1-wave argues against this solution.

As remarked above solutions I and II are both continuations of solution A_{I^-} of Bland et al.[1]. From the present analysis alone there is no way of distinguishing between them. Indications of a slight preference for solution II can be derived from the $K^+p \rightarrow KN\pi$ channel as analysed by Bland et al.[11]. In this analysis there is preference for a small S_1-wave which would be in agreement with the large elasticity observed in the S_1-wave of our solution II and in disagreement with solution I.

Perhaps the most striking feature of both solution I and II is the counterclockwise half circle described by the P_3-wave. This behaviour is also seen in the KN* analysis of Bland et al.[11], who find the same half circle apart from a phase factor. The D_3 amplitude remains small at all momenta, whereas one would have expected that both KN* and K*N go dominantly through this partial wave. The D_5-wave gives an important contribution to the inelastic cross-section. This can account for the non-zero A_4 coefficient in the KN* production angular distribution[11].

Acknowledgements

The authors would like to thank Drs. C. Lovelace and C. Schmid for discussions. The contribution of J. Conciencia, O. Runolfsson, M. Uldry, and J. Vermeulen of the polarized target group has been vital for the success of the experiment. We are indebted to M. Arbet for technical assistance in the course of this experiment. This work was supported in part by the Stichting voor Fundamenteel Onderzoek der Materie (F.O.M.), which is supported by the Nederlandse Organisatie voor Zuiver Wetenschappelijk Onderzoek (Z.W.O.).

REFERENCES

1) R.W. Bland, G. Goldhaber, B.H. Hall, J.A. Kadyk, V.H. Seeger, G.H. Trilling and C.G. Wohl, UCRL-18323.

2) A.T. Lea, B.R. Martin and G.C. Oades, Phys.Rev. 165, 1770 (1968).

3) S. Andersson, C. Daum, F.C. Erné, J.P. Lagnaux, J.C. Sens and F. Udo, Phys.Letters 28 B, 611 (1969).

4) S. Mango, O. Runolfsson and M. Borghini, submitted to Nuclear Instrum. Methods.

5) C. Lovelace and F. Wagner, 14th Int.Conf. on High-Energy Physics, Vienna (1968) (CERN, Geneva, 1968), abstract 254.

6) S. Goldhaber et al., Phys.Rev.Letters 9, 135 (1962). Differential cross-sections at 140, 175, 205, 235, 265, 355, 520 and 642 MeV/c.
T.F. Kycia et al., Phys.Rev. 118, 553 (1960). Differential and total cross-sections at 523 MeV/c.
E. Barrelet (private communication, V. Henri). Differential cross-section at 735 MeV/c.
S. Focardi et al., Phys.Rev.Letters 7, 188 (1961). Differential cross-section at 810 MeV/c.
T.F. Stubbs et al., Phys.Rev.Letters 7, 188 (1961). Differential cross-section at 810 MeV/c.
R.W. Bland et al., UCRL-18131 (1968). Differential and inelastic cross-sections 865, 970, 1215, 1367 MeV/c.
W. Hirsch et al., Phys.Rev. 135 B, 191 (1964). Differential cross-section at 910 MeV/c.
V. Cook et al., Phys.Rev. 129, 2743 (1963). Differential cross-sections at 970, 1170, 1970 MeV/c.
A.S. Carrol et al., Phys.Rev.Letters 21, 1282 (1968) and private communication. Backward differential cross-sections from 993 to 2451 MeV/c.
A. Bettini et al., Phys.Letters 16, 83 (1965). Differential cross-section at 1455 MeV/c.

7) R.L. Cool et al., Phys.Rev.Letters 17, 102 (1966).
D.V. Bugg et al., Phys.Rev. 168, 1466 (1968).

8) A. Carter, Rutherford report, REHL-68/10 (1968) (with a 25% error).

9) C.H. Johnson and H.M. Steiner, UCRL-18001 (1967).

10) C. Schmid, private communication.

11) R.W. Bland, thesis, UCRL-18131 (1968).

Captions to Tables 1-6

K^+p polarization and differential cross-section data with errors. In the polarization data the statistical errors are indicated. The differential cross-section data have been normalized to existing data[6]. Their statistical errors have been doubled to account for systematic errors. There is an additional scale uncertainty of 15%. The polarization data at 1.22 GeV/c of Ref. 3 have been multiplied by 0.85 to account for an error in the target polarization.

Table 1

Incident momentum 865 MeV/c

$\cos\theta_{c.m.}$	Polarization	$d\sigma/d\Omega$(mb/sr)
0.79	0.61 ± 0.24	1.04 ± 0.19
0.70	0.70 ± 0.12	1.31 ± 0.19
0.64	0.23 ± 0.28	0.88 ± 0.23
0.59	0.49 ± 0.24	1.05 ± 0.22
0.53	0.85 ± 0.17	0.84 ± 0.20
0.48	0.52 ± 0.27	0.88 ± 0.20
0.42	0.49 ± 0.17	1.01 ± 0.31
0.37		0.93 ± 0.23
0.33	0.94 ± 0.16	
0.31		1.05 ± 0.24
0.25	0.69 ± 0.29	
0.20	0.50 ± 0.25	
0.18		0.78 ± 0.08
0.14	0.85 ± 0.29	
0.06	0.77 ± 0.18	0.71 ± 0.10
-0.03	0.45 ± 0.17	0.87 ± 0.13
-0.11	0.70 ± 0.16	0.86 ± 0.12
-0.21	0.10 ± 0.14	0.90 ± 0.11
-0.29	0.79 ± 0.18	0.89 ± 0.13
-0.36	0.34 ± 0.16	0.79 ± 0.11
-0.43	0.53 ± 0.19	0.80 ± 0.13
-0.50	0.45 ± 0.17	0.85 ± 0.12
-0.57	0.47 ± 0.18	0.85 ± 0.12
-0.64	0.32 ± 0.18	0.86 ± 0.13
-0.72	0.15 ± 0.15	1.00 ± 0.12
-0.81	0.34 ± 0.24	0.88 ± 0.18

Table 2

Incident momentum 971 MeV/c

$\cos\theta_{c.m.}$	Polarization	$d\sigma/d\Omega$(mb/sr)
0.83	0.82 ± 0.23	0.96 ± 0.17
0.74	0.71 ± 0.09	1.15 ± 0.15
0.65	0.76 ± 0.10	1.24 ± 0.15
0.60		1.22 ± 0.21
0.55		1.11 ± 0.20
0.50	0.77 ± 0.11	0.99 ± 0.19
0.44		1.10 ± 0.22
0.40	0.63 ± 0.11	
0.38		0.91 ± 0.18
0.29	0.85 ± 0.13	
0.20	0.63 ± 0.15	
0.17		0.89 ± 0.10
0.12	0.64 ± 0.17	
0.03	0.93 ± 0.23	0.79 ± 0.22
-0.02		0.88 ± 0.24
-0.05	0.62 ± 0.14	
-0.08		0.85 ± 0.17
-0.15	0.34 ± 0.13	0.80 ± 0.10
-0.23	0.43 ± 0.15	0.82 ± 0.12
-0.31	0.49 ± 0.13	0.82 ± 0.09
-0.38	0.36 ± 0.16	0.72 ± 0.10
-0.45	0.23 ± 0.13	0.84 ± 0.10
-0.53	0.35 ± 0.15	0.74 ± 0.10
-0.60	0.31 ± 0.15	0.85 ± 0.11
-0.66	0.37 ± 0.15	0.87 ± 0.11
-0.72	0.17 ± 0.17	0.83 ± 0.12
-0.78	-0.13 ± 0.16	0.87 ± 0.13
-0.84	0.09 ± 0.25	0.90 ± 0.21

Table 3

Incident momentum 1087 MeV/c

$\cos\theta_{c.m.}$	Polarization	$d\sigma/d\Omega$(mb/sr)
0.85	0.75 ± 0.16	1.24 ± 0.17
0.78	0.71 ± 0.10	1.39 ± 0.16
0.71	0.60 ± 0.09	1.39 ± 0.14
0.63	0.55 ± 0.09	0.98 ± 0.17
0.54	0.68 ± 0.09	1.04 ± 0.09
0.46	0.90 ± 0.19	0.87 ± 0.14
0.41	0.69 ± 0.12	0.92 ± 0.12
0.35	0.90 ± 0.10	0.80 ± 0.14
0.29	0.90 ± 0.24	0.92 ± 0.30
0.23	0.62 ± 0.26	0.83 ± 0.20
0.14	0.82 ± 0.36	0.60 ± 0.26
0.06	1.21 ± 0.56	0.50 ± 0.25
-0.04	0.74 ± 0.16	0.49 ± 0.08
-0.11	0.85 ± 0.18	0.55 ± 0.09
-0.16		0.45 ± 0.11
-0.19	0.79 ± 0.15	
-0.23		0.49 ± 0.06
-0.29	0.67 ± 0.22	
-0.35	0.42 ± 0.16	0.46 ± 0.06
-0.43	0.41 ± 0.15	0.50 ± 0.06
-0.51	0.07 ± 0.22	0.41 ± 0.06
-0.58	0.13 ± 0.19	0.50 ± 0.07
-0.64	0.64 ± 0.17	0.52 ± 0.07
-0.72	0.28 ± 0.14	0.51 ± 0.06
-0.81	-0.13 ± 0.16	0.51 ± 0.07

Table 4

Incident momentum 1215 MeV/c

$\cos\theta_{c.m.}$	Polarization	$d\sigma/d\Omega$(mb/sr)
0.83	0.54 ± 0.09	1.42 ± 0.25
0.77	0.60 ± 0.06	1.66 ± 0.19
0.70	0.65 ± 0.05	1.78 ± 0.18
0.60	0.71 ± 0.04	1.38 ± 0.13
0.50	0.60 ± 0.06	1.28 ± 0.15
0.39	0.73 ± 0.06	0.95 ± 0.10
0.32	0.68 ± 0.09	0.73 ± 0.12
0.25	0.75 ± 0.08	0.78 ± 0.12
0.18	0.54 ± 0.08	0.77 ± 0.12
0.12	0.82 ± 0.10	0.45 ± 0.07
0.05	0.63 ± 0.09	0.50 ± 0.09
-0.01	0.72 ± 0.10	0.53 ± 0.10
-0.07	0.75 ± 0.12	0.37 ± 0.07
-0.16	0.48 ± 0.09	0.57 ± 0.10
-0.26	0.48 ± 0.11	0.38 ± 0.07
-0.35	0.35 ± 0.13	0.40 ± 0.10
-0.46	0.09 ± 0.14	0.30 ± 0.07
-0.55	0.23 ± 0.10	0.42 ± 0.07
-0.66	0.12 ± 0.14	0.40 ± 0.09
-0.74	0.01 ± 0.13	0.25 ± 0.06
-0.82	0.04 ± 0.19	0.35 ± 0.12

Table 5

Incident momentum 1372 MeV/c

$\cos\theta_{c.m.}$	Polarization	$d\sigma/d\Omega$(mb/sr)
0.87	0.42 ± 0.11	1.76 ± 0.17
0.80	0.56 ± 0.07	1.77 ± 0.16
0.73	0.48 ± 0.08	1.65 ± 0.22
0.68	0.55 ± 0.12	1.51 ± 0.20
0.63		1.36 ± 0.19
0.60	0.68 ± 0.08	
0.57		1.16 ± 0.15
0.52	0.48 ± 0.10	1.09 ± 0.12
0.45	0.70 ± 0.12	0.95 ± 0.13
0.37	0.67 ± 0.09	
0.28	0.62 ± 0.13	
0.20	0.72 ± 0.60	
0.14		0.49 ± 0.07
−0.06	0.71 ± 0.24	
−0.13	0.92 ± 0.27	
−0.18		0.36 ± 0.07
−0.21	0.37 ± 0.20	
−0.24		0.31 ± 0.10
−0.29	0.62 ± 0.23	0.32 ± 0.05
−0.36	0.44 ± 0.20	0.28 ± 0.05
−0.44	0.23 ± 0.23	0.22 ± 0.05
−0.52	0.39 ± 0.20	0.27 ± 0.05
−0.59	0.16 ± 0.25	0.22 ± 0.05
−0.65	0.04 ± 0.24	0.25 ± 0.05
−0.71	−0.06 ± 0.13	0.24 ± 0.05
−0.79	0.17 ± 0.23	0.22 ± 0.04
−−0.36	−0.45 ± 0.47	0.22 ± 0.09

Table 6

Incident momentum 1453 MeV/c

$\cos\theta_{c.m.}$	Polarization	$d\sigma/d\Omega$(mb/sr)
0.89	00.45 ± 0.11	
0.86		1.98 ± 0.19
0.82	0.59 ± 0.06	
0.77	0.58 0.12	1.79 ± 0.17
0.70	0.55 ± 0.06	1.68 ± 0.22
0.66		1.55 ± 0.20
0.61	0.60 ± 0.08	1.30 ± 0.18
0.55	0.48 ± 0.09	1.17 ± 0.12
0.46	0.79 ± 0.08	1.02 ± 0.09
0.38	0.70 ± 0.11	0.72 ± 0.09
0.31	0.82 ± 0.16	0.67 ± 0.14
0.25	0.96 ± 0.36	
0.19	0.53 ± 0.53	
0.14	1.07 ± 0.44	0.48 ± 0.07
0.07	0.34 ± 0.33	
-0.02	0.50 ± 0.65	
-0.10	0.60 ± 0.20	
-0.15		0.41 ± 0.08
-0.18	0.60 ± 0.14	
-0.21		0.32 ± 0.07
-0.27	0.69 ± 0.18	0.30 ± 0.06
-0.35	0.40 ± 0.19	0.30 ± 0.05
-0.42	0.10 ± 0.90	0.21 ± 0.04
-0.50	0.46 ± 0.24	0.20 ± 0.04
-0.57	0.84 ± 0.30	0.16 ± 0.04
-0.64	-0.03 ± 0.28	0.15 ± 0.04
-0.70	-0.24 ± 0.32	0.14 ± 0.04
-0.76	0.34 ± 0.37	0.20 ± 0.06
-0.83	0.14 ± 0.44	0.21 ± 0.04

Table 7

$K^+p \rightarrow K^+p$ shortest path solutions

Momentum (MeV/c)	c.m. energy (MeV)	Re or Im part	SOLUTION I					SOLUTION II					SOLUTION III				
			S_1 $\times 10^{-2}$	P_1 $\times 10^{-2}$	P_3 $\times 10^{-2}$	D_3 $\times 10^{-2}$	D_5 $\times 10^{-2}$	S_1 $\times 10^{-2}$	P_1 $\times 10^{-2}$	P_3 $\times 10^{-2}$	D_3 $\times 10^{-2}$	D_5 $\times 10^{-2}$	S_1 $\times 10^{-2}$	P_1 $\times 10^{-2}$	P_3 $\times 10^{-2}$	D_3 $\times 10^{-2}$	D_5 $\times 10^{-2}$
140	1445	Re	−12	0	0	0	0	−12	0	0	0	0	–	–	–	–	–
		Im	2	0	0	0	0	2	0	0	0	0	–	–	–	–	–
175	1452	Re	−17	0	0	0	0	−17	0	0	0	0	2	7	−14	0	0
		Im	3	0	0	0	0	3	0	0	0	0	0	1	2	0	0
205	1459	Re	−18	0	0	0	0	−18	0	0	0	0	2	8	−14	0	0
		Im	3	0	0	0	0	3	0	0	0	0	0	1	2	0	0
235	1466	Re	−20	0	0	0	0	−20	0	0	0	0	2	9	−14	0	0
		Im	4	0	0	0	0	4	0	0	0	0	0	1	2	0	0
265	1475	Re	−23	−1	1	0	0	−23	−1	1	0	0	0	10	−17	0	0
		Im	6	0	0	0	0	6	0	0	0	0	0	1	3	0	0
355	1505	Re	−31	−4	2	0	0	−31	−4	2	0	0	0	13	−22	0	0
		Im	11	0	0	0	0	11	0	0	0	0	0	2	6	0	0
520	1572	Re	−42	−9	4	0	0	−42	−9	4	0	0	−1	19	−31	0	0
		Im	25	1	2	0	0	25	1	2	0	0	1	4	12	0	0
642	1626	Re	−46	−10	6	0	0	−46	−10	6	0	0	0	22	−35	0	0
		Im	33	1	1	0	0	33	1	1	0	0	0	5	15	0	0
735	1669	Re	−46	−10	8	−6	3	−46	−10	8	−6	3	0	23	−37	2	1
		Im	34	1	1	1	0	34	1	1	1	0	0	6	16	0	0
778	1689	Re	−48	−12	10	−4	0	−48	−12	10	−4	0	−1	23	−38	0	1
		Im	40	2	1	0	0	40	2	1	0	0	0	7	18	0	0
820	1704	Re	−48	−13	12	−6	0	−48	−13	12	−6	0	−1	25	−41	0	2
		Im	44	3	2	9	0	44	3	2	1	0	1	8	22	1	0
865	1730	Re	−50	−17	14	−6	−2	−49	−14	14	−6	−2	−26	6	−37	−6	20
		Im	50	3	2	1	1	49	2	4	1	0	8	0	18	1	5
910	1751	Re	−49	−22	14	−6	0	−49	−17	10	−2	−1	−34	8	−37	−6	20
		Im	57	6	2	1	1	50	5	4	1	1	18	2	18	1	4
971	1780	Re	−37	−19	14	−4	2	−45	−13	14	−6	4	−29	5	−30	−6	22
		Im	56	6	2	0	5	51	2	7	3	3	14	0	22	0	8
1087	1834	Re	−28	−24	12	−6	0	−42	−12	10	−7	4	−34	0	−30	−7	19
		Im	64	11	6	1	6	53	2	15	5	4	18	0	26	1	12
1170	1873	Re	−21	−26	5	−6	−9	−41	−18	7	−11	2	−34	−3	−33	−6	14
		Im	67	8	18	2	6	58	6	21	6	4	26	1	30	1	14
1217	1893	Re	−8	−23	0	−14	−3	−48	−17	4	−10	3	−36	−4	−29	−6	17
		Im	74	6	14	2	7	62	5	19	4	7	29	3	27	2	14
1367	1963	Re	−2	−25	1	−14	−2	−49	−22	2	−6	7	−43	−8	−27	−6	17
		Im	77	10	21	3	9	58	10	22	9	11	33	7	30	4	18
1453	2002	Re	−2	−32	−2	−16	−6	−49	−24	2	−7	7	−46	−10	−24	−6	14
		Im	72	14	25	4	10	49	12	26	11	13	33	8	32	5	19

Figure captions

Fig. 1 : Differential cross-section and polarization data at 865, 971, and 1087 MeV/c. Curves from phase-shift fits: —— solutions I, II; --- solution III.

Fig. 2 : Differential cross-section and polarization data at 1215, 1372, and 1453 MeV/c. Curves from phase-shift fits: —— solutions I, II; --- solution III.

Fig. 3 : Regions where 200 phase-shift solutions at 865 MeV/c are found after 470 random searches.

Fig. 4 : Regions where 200 phase-shift solutions at 1215 MeV/c are found after 460 random searches.

Fig. 5 : Argand plot of the S_1 wave for three shortest path solutions from threshold up to 1.45 GeV/c: -- solution I; —— solution II; ----- solution III. The symbol O indicates a momentum where differential cross-section and polarization data are available. The symbol ● a momentum with only differential cross-section data.

Fig. 6 : Argand plot for the P_1 wave, etc.

Fig. 7 : Argand plot for the P_3 wave, etc.

Fig. 8 : Argand plot for the D_3 wave, etc.

Fig. 9 : Argand plot for the D_5 wave, etc.

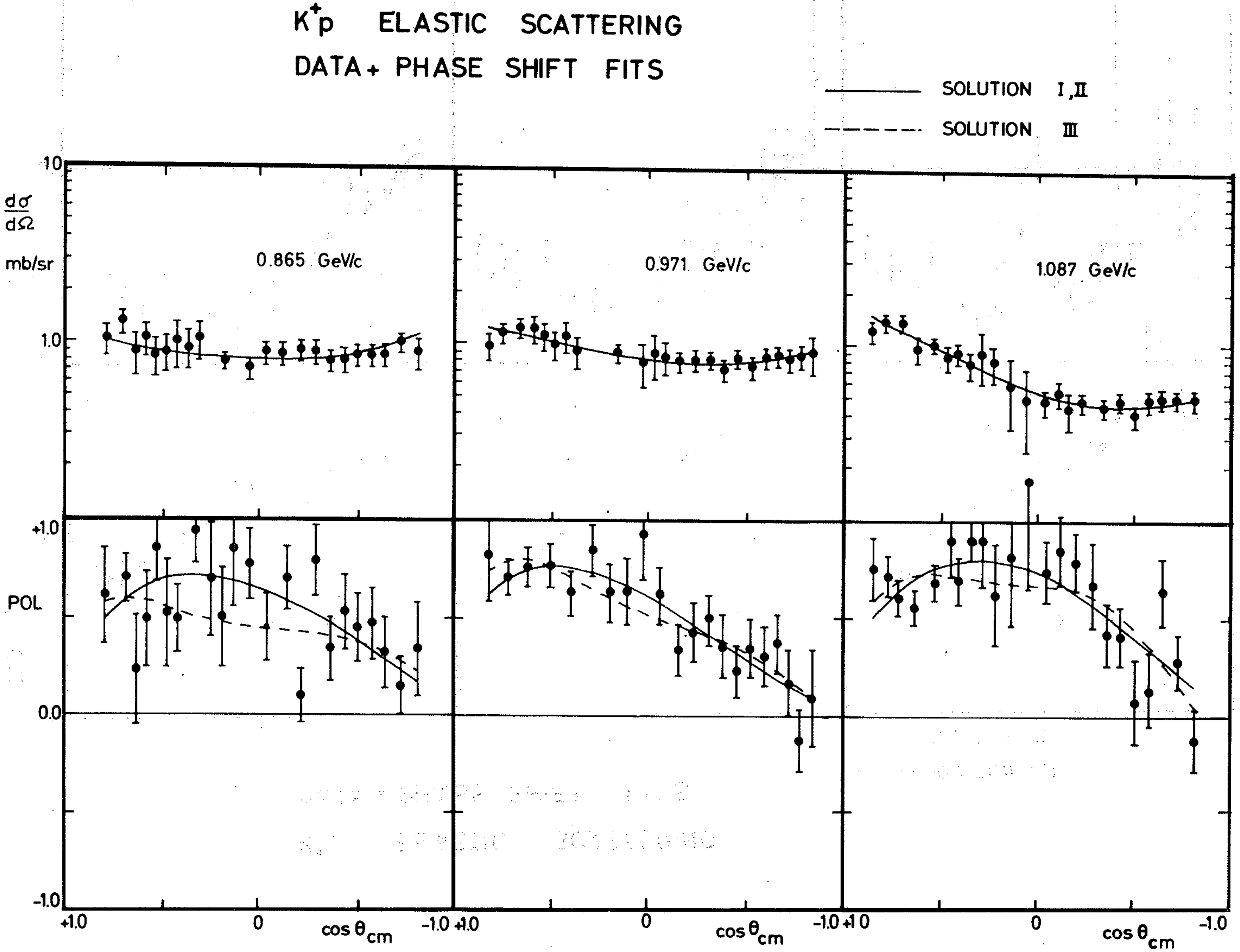

K⁺p ELASTIC SCATTERING
DATA + PHASE SHIFT FITS
SOLUTION I,II
SOLUTION III
dσ/dΩ
mb/sr
10
1.0
0.865 GeV/c
0.971 GeV/c
1.087 GeV/c
POL
+1.0
0.0
-1.0
+1.0
0
cos θcm
-1.0

Fig. 1

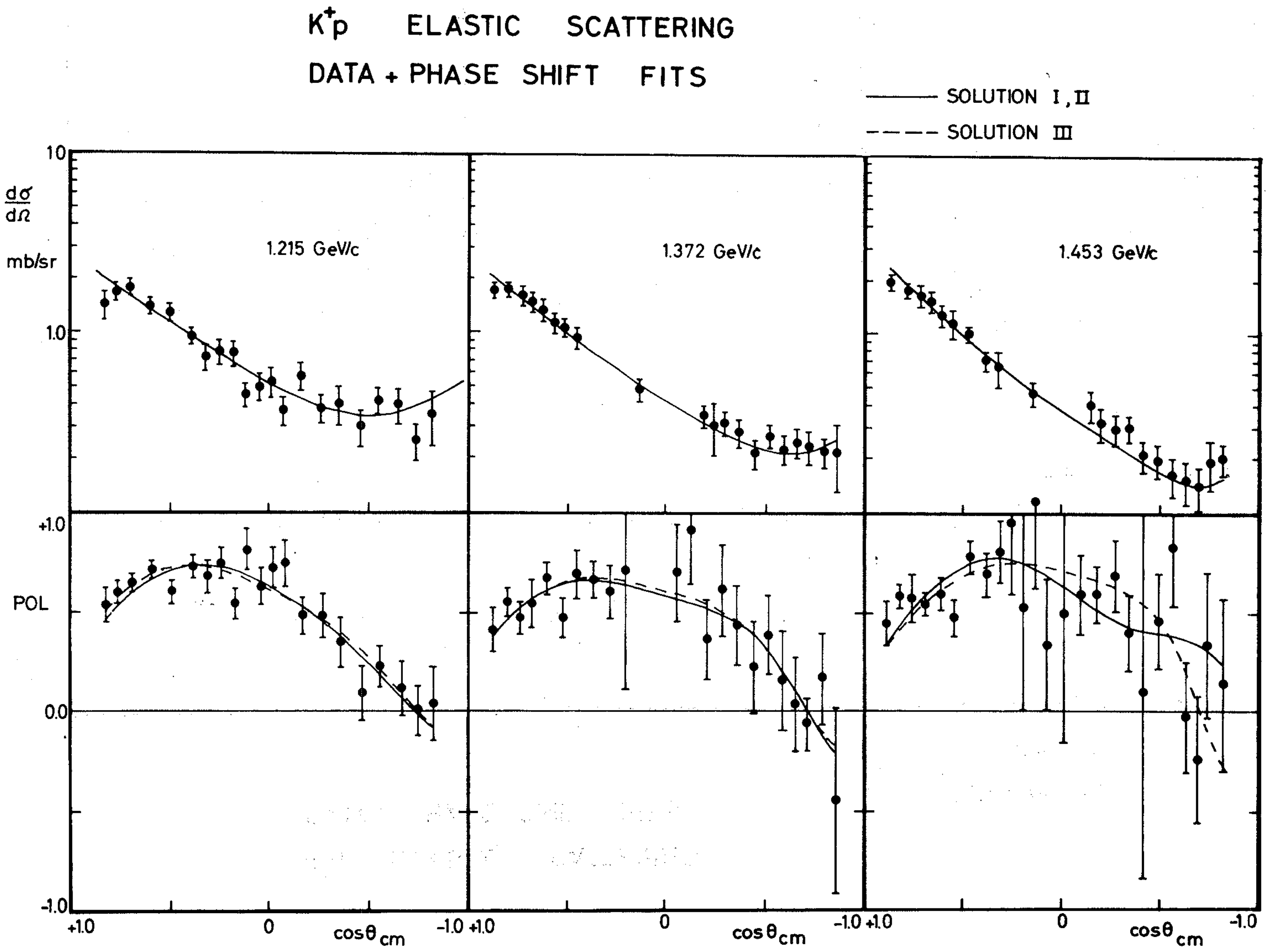

K+p ELASTIC SCATTERING
DATA + PHASE SHIFT FITS
SOLUTION I, II
SOLUTION III
dσ/dΩ
mb/sr
10
1.0
1.215 GeV/c
1.372 GeV/c
1.453 GeV/c
+1.0
POL
0.0
-1.0
+1.0
0
cosθcm
-1.0

Fig. 2

$K^+p \longrightarrow K^+p$

200 PHASE SHIFT SOLUTIONS AT 865 MeV/c

FROM 470 RANDOM SEARCHES

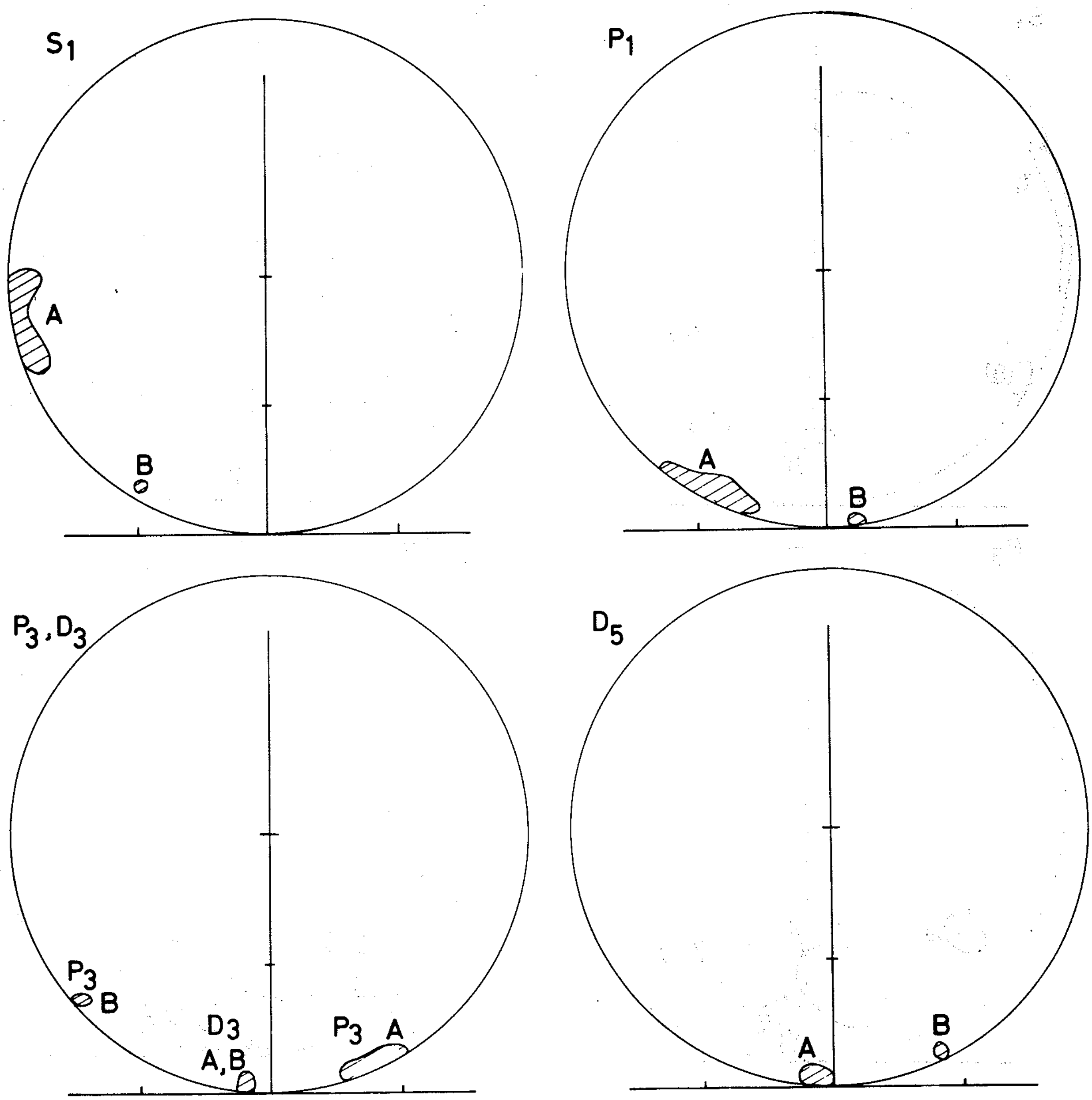

Fig. 3

200 PHASE SHIFT SOLUTIONS AT 1.215 GeV/c
FROM 460 RANDOM SEARCHES

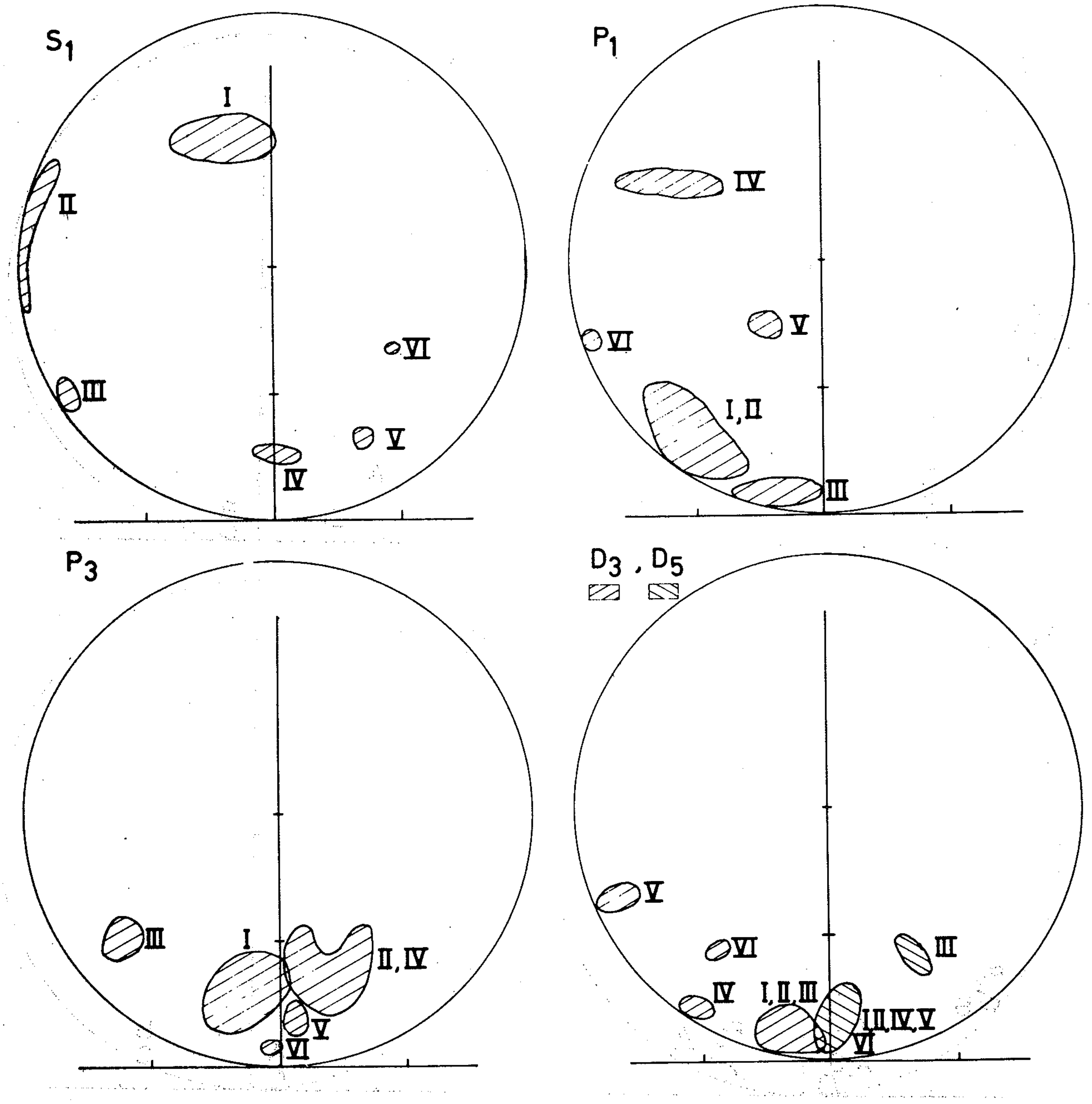

Fig. 4

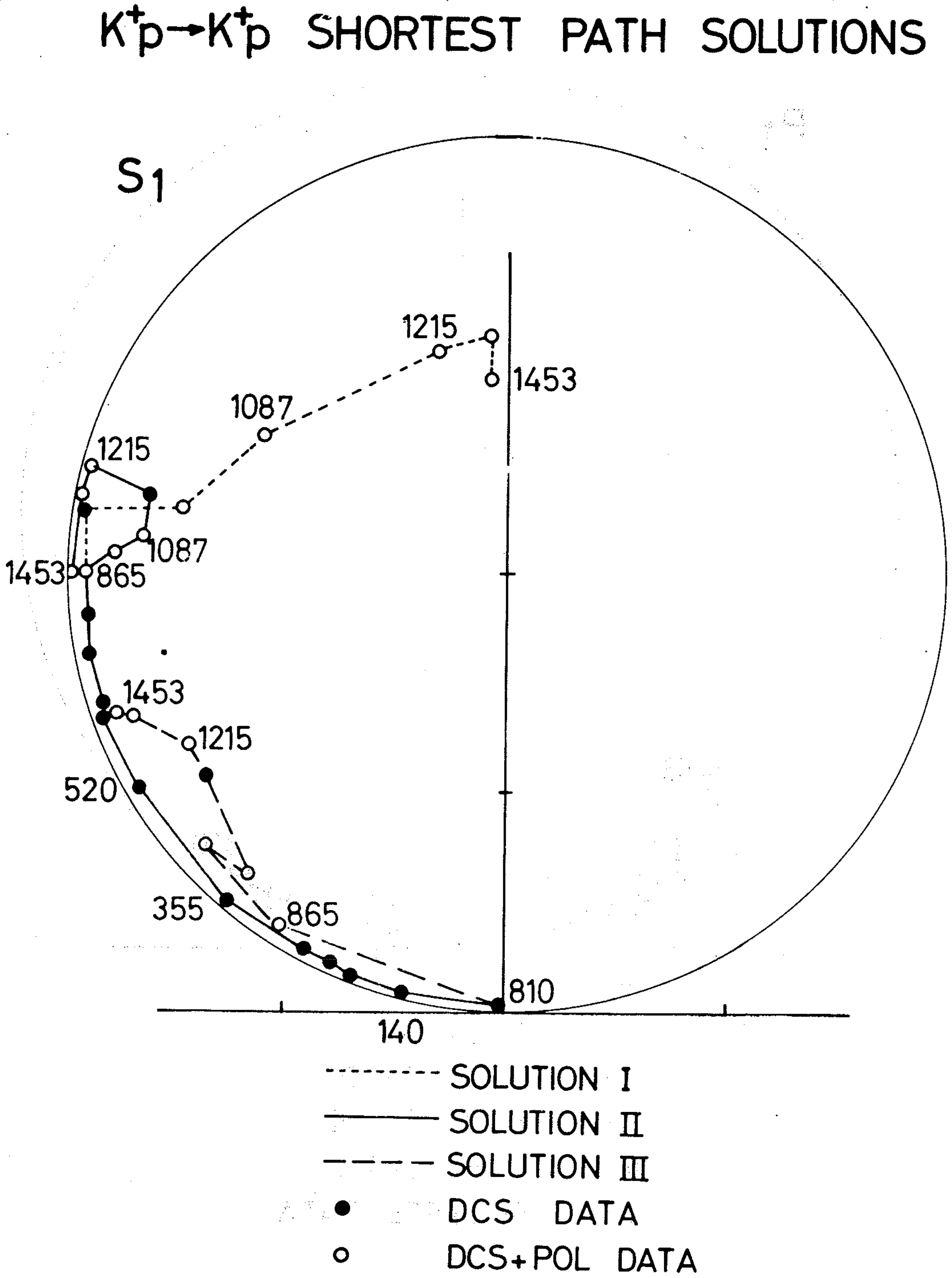
K⁺p→K⁺p SHORTEST PATH SOLUTIONS
S1
1215
1453
1087
1215
1087
1453
865
1453
1215
520
355
865
810
140
SOLUTION I
SOLUTION II
SOLUTION III
DCS DATA
DCS+POL DATA

Fig. 5

$K^+p \rightarrow K^+p$ SHORTEST PATH SOLUTIONS

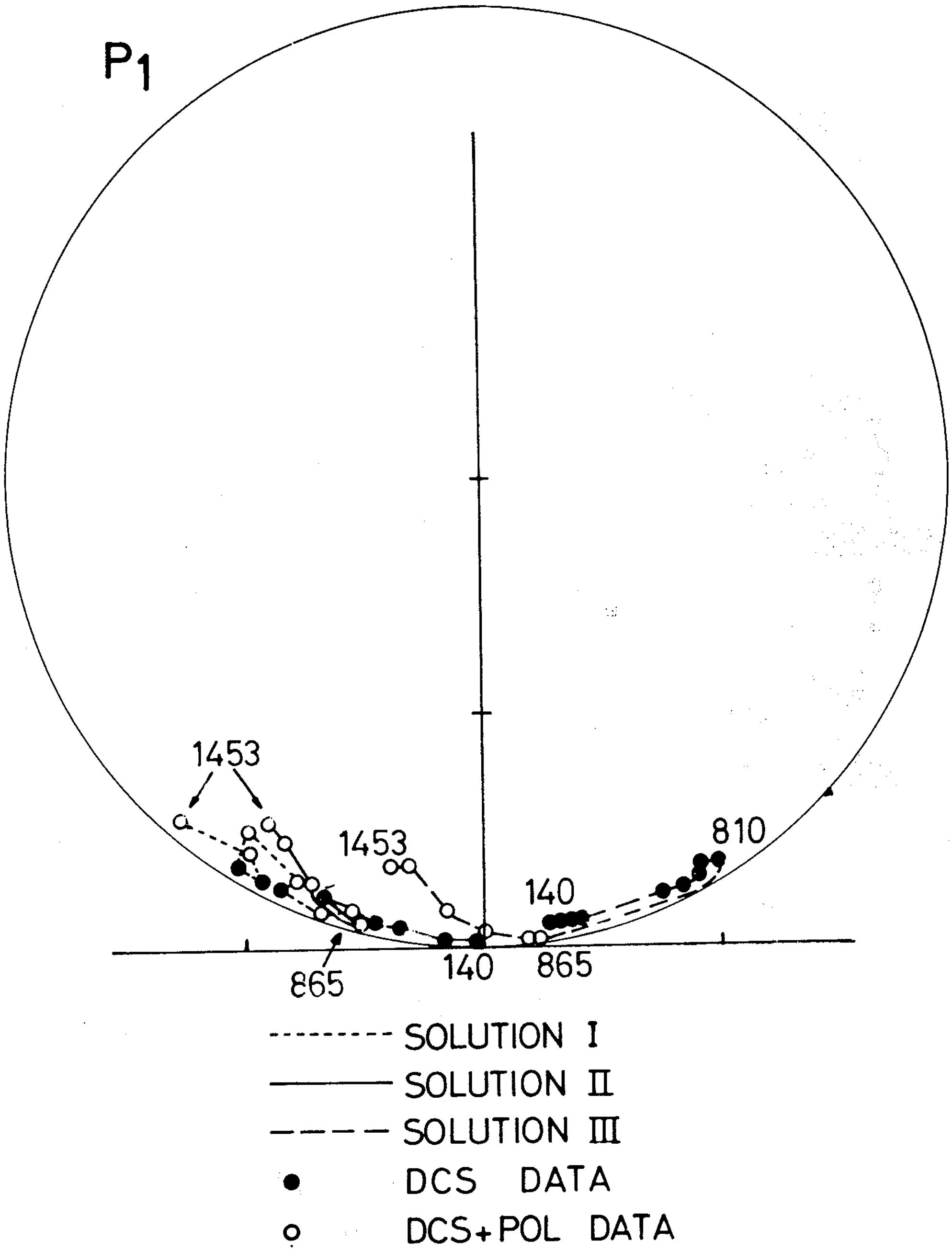

Fig. 6

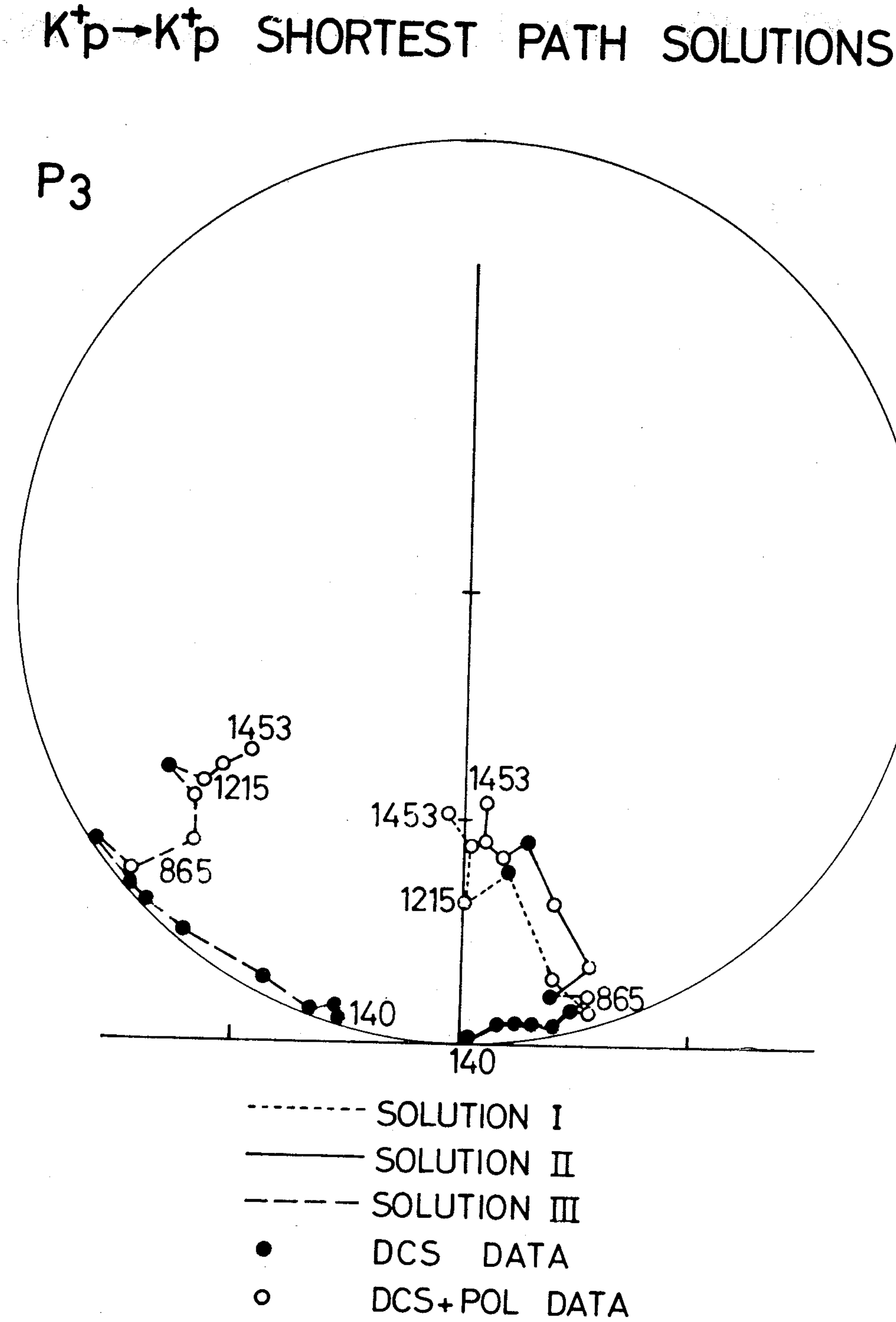

K⁺p→K⁺p SHORTEST PATH SOLUTIONS
P3
1453
1215
865
140
1453
1453
1215
865
140
SOLUTION I
SOLUTION II
SOLUTION III
DCS DATA
DCS+POL DATA

Fig. 7

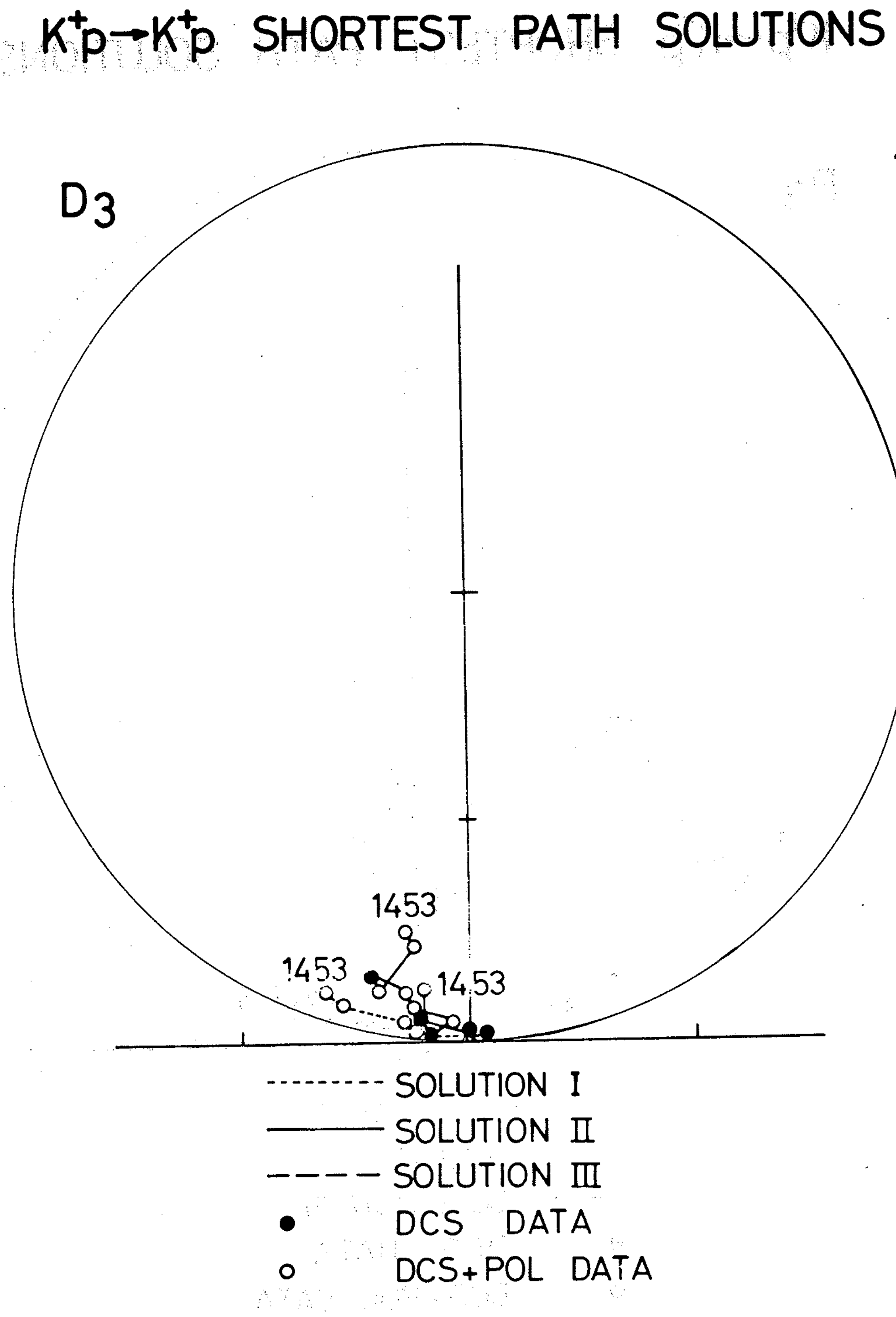

K⁺p→K⁺p SHORTEST PATH SOLUTIONS
D3
1453
1453
1453
SOLUTION I
SOLUTION II
SOLUTION III
DCS DATA
DCS+POL DATA

Fig. 8

$K^+p \to K^+p$ SHORTEST PATH SOLUTIONS

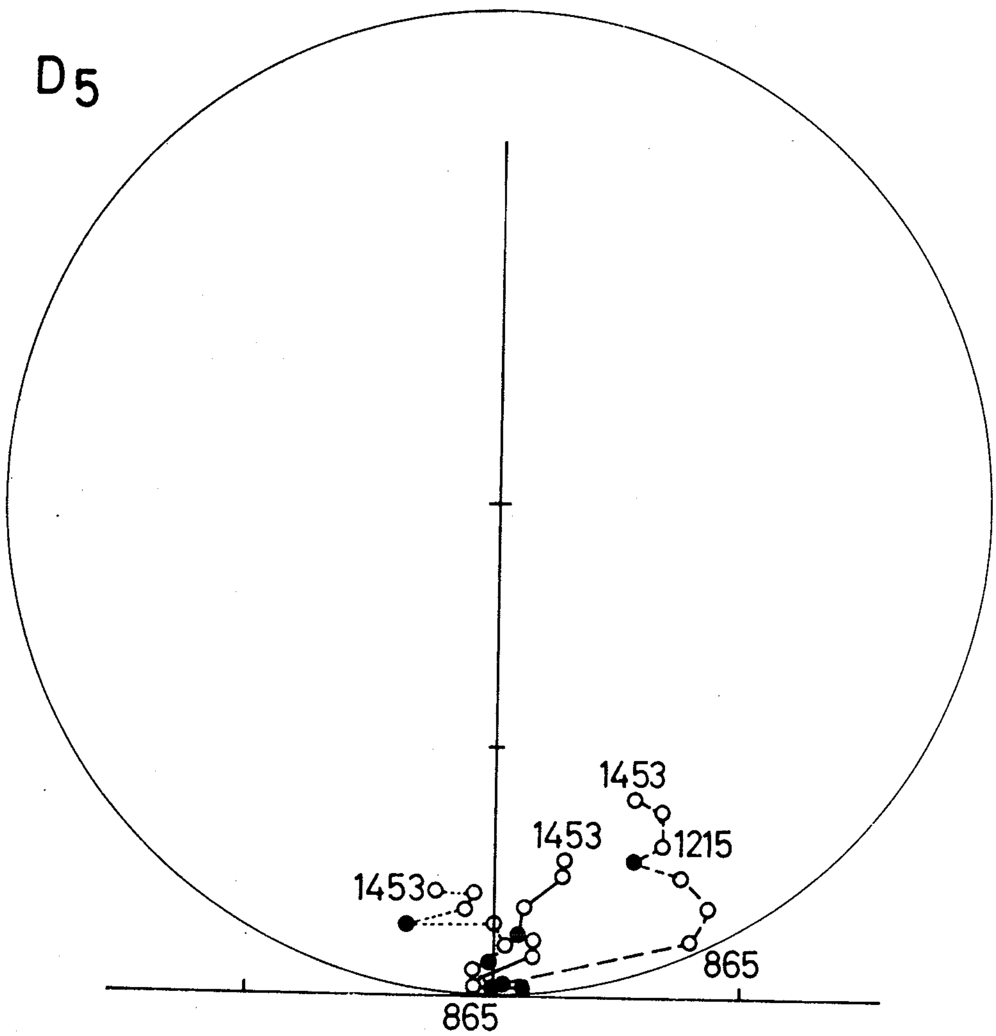

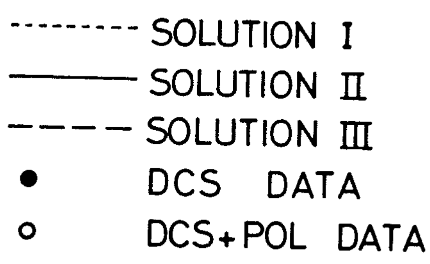

Fig. 9